

Low volumes of quartz cement in deeply buried Fulmar Formation sandstones explained by a low effective stress burial history

Olakunle J. Oye^{a,b,*}, Andrew C. Aplin^a, Ian J. Orland^{c,d}, John W. Valley^c

^a Department of Earth Sciences, Durham University, Durham, DH1 3LE, UK

^b Geoscience Division, Degeconek Limited, Lagos, Nigeria

^c WiscSIMS Lab, Dept. of Geoscience, Univ. of Wisconsin, Madison, WI, 53706, USA

^d Wisconsin Geological and Natural History Survey, University of Wisconsin, Madison, WI, 53705, USA

ARTICLE INFO

Keywords:

Sandstone
Grain fracturing
Quartz cement
Effective stress
Intergranular pressure dissolution
Secondary ion mass spectrometry
Oxygen isotopes

ABSTRACT

Upper Jurassic Fulmar Formation sandstones from the Fulmar Field in the Central North Sea are buried to 3.2 km and 128 °C but contain only $3.7 \pm 1.7\%$ (1σ) quartz cement, substantially less than volumes predicted by models based on temperature-related quartz precipitation kinetics. Oxygen isotope microanalysis of quartz overgrowths suggests that only limited cementation occurred at temperatures above 110 °C. We suggest that the anomalously low volumes of quartz cement are most readily explained by the effective stress history of the Fulmar Formation. Regional pore pressure analysis strongly suggests that pore fluid pressures in the Fulmar Formation decreased substantially in the last <0.5 Ma as a result of lateral seal failure, increasing effective stress from ca. 10 MPa to the current 31 MPa. A recent increase in effective stress is supported by the common occurrence of grains that are both fractured and unhealed by quartz cement. Intergranular pressure dissolution can account for around one third of the observed quartz cement, with the remainder from deep burial feldspar dissolution. We argue that the continuous history of low effective stress, until the very recent geological past, limited the rate of silica supply by intergranular pressure dissolution, and thus the rate of quartz cementation. Effective stress histories should be incorporated into predictive models of quartz cementation of sandstones.

1. Introduction

Sandstone reservoir quality (porosity and permeability) is one of the main criteria for assessing the likelihood of exploration, production and fluid injection success in a clastic setting. Understanding the processes that control porosity evolution in sandstones is thus important for the accurate prediction of pore to reservoir-scale quality related to the production, storage and injection of hydrocarbon and other fluids.

Quartz cement is the most important porosity reducing cement in sandstones (McBride, 1989; Worden et al., 2018). As sands undergo burial and transform to sandstone, vertical effective stress (VES, i.e. vertical stress minus pore pressure) drives porosity reduction by controlling the extent of mechanical compaction at shallow depth (<2500 m and temperature <80 °C) and influencing the degree of chemical compaction/intergranular pressure dissolution of quartz (IPD; e.g. van Noort et al., 2008). Because vertical effective stress reduces as pore pressure increases at a given depth, changes in pore pressure affects the susceptibility of sediments to compaction, pressure dissolution, and

cementation.

Under hydrostatic condition, vertical effective stress increases linearly with increasing burial. However, basin subsidence can be punctuated by intermittent episodes of pore pressure inflation and/or deflation events triggered by a range of mechanisms (Osborne and Swarbrick, 1997; Swarbrick et al., 2005), thus complicating pore pressure and VES histories. Unlike temperature history, for which paleothermometers such as vitrinite reflectance can reveal historical thermal fluctuations, there are no similar palaeo-tools for assessing variations in stress evolution through time. Hence, it is often difficult to reconstruct accurate VES histories from basin models (Oye et al., 2020). This makes it difficult to accurately assess the impact of VES on IPD and quartz cementation in diagenetic studies. Previous research (Laubach, 1989; Makowitz and Milliken, 2003; Worden et al., 2018; Zeng, 2010) suggests that grain fractures (also known as microfractures) can be good indicators of palaeostress and can form in sandstones during early diagenesis and continue to the mesogenesis stage. Fracture cross-cutting relations, along with fluid inclusion and/or oxygen isotope data from

* Corresponding author. Geoscience Division, Degeconek Limited, Lagos, Nigeria.

E-mail address: lakunleoye@yahoo.co.uk (O.J. Oye).

<https://doi.org/10.1016/j.geoen.2022.211383>

Received 8 July 2022; Received in revised form 5 November 2022; Accepted 19 December 2022

Available online 20 December 2022

2949-8910/© 2022 The Authors. Published by Elsevier B.V. This is an open access article under the CC BY license (<http://creativecommons.org/licenses/by/4.0/>).

fracture-filling cement, are some of the tools that can be used to infer the relative timing of fracture formation (Zeng, 2010) and inflection points in stress and temperature histories.

One of the known causes of grain fracturing is increased vertical effective stress due to vertical loading from sediment overburden (Makowitz and Milliken, 2003; Worden et al., 2018). Framework grain fracturing can manifest in quartz-rich sandstone reservoirs in response to increased vertical effective stress following a rapid pore pressure reduction triggered by seal failure or anthropogenic activities like hydrocarbon or geothermal fluid production (DiGiovanni et al., 2007; Pijenburg et al., 2019; Teufel et al., 1991; Verberne et al., 2021). This includes sandstones that are deeply buried but in which fluid pressures have remained high through the deeper part of their burial history, such that effective stress has remained low. As such, integration of grain fracture data from petrographic studies of sandstones with their stress history, should provide insights into the VES pathway through time, and a more accurate assessment of the role of VES on intergranular pressure dissolution and quartz cementation.

Here, we report a detailed study of the Fulmar Formation in the Fulmar Field, UK Central North Sea. Buried to 130 °C and with a present-day pore pressure that is only 7 MPa above hydrostatic, these sandstones have low volumes of quartz cement that, at first sight, cannot be readily explained either by stress-related IPD or by temperature-driven cementation models (Lander and Walderhaug, 1999; Walderhaug, 1994a, 1996). However, modelling of regional pore pressure data from the Fulmar, and proximal Clyde and Halley fields (Swarbrick et al., 2005), suggests a rapid deflation of pore pressure in the Fulmar Formation sands in this area, over the last ca. 0.5 million years. This unusual pore pressure/VES history allows us to explore the role of VES history on IPD and quartz cementation. We integrate (a) detailed petrographic analysis, (b) basin modelling to understand the burial, temperature, and vertical effective stress histories, (c) high spatial resolution oxygen isotope analysis of quartz cement and (d) a kinetic model of quartz cementation to suggest that VES history plays a key role in quartz cementation of sandstones through its control on the rate of supply of silica through intergranular pressure dissolution.

2. Geological setting

This study is focussed on Upper Jurassic Fulmar Formation sands from the Fulmar Field, located in the United Kingdom sector of the Central North Sea in Blocks 30/16 and 30/11b (Fig. 1). The Fulmar structure is a product of halokinesis, basement fault reactivation and syn – post depositional fault movement (Kuhn et al., 2003), leading to the deposition of the sedimentary units outlined in Table 1. A simple stratigraphy of the Fulmar Field is shown on Fig. 2. The Late Jurassic, shallow marine Fulmar Formation is a thick (>100 m), laterally continuous shoreface sandstone that occurs across the Fulmar-Clyde-Halley region. The formation, compartmentalized by faulting, comprises mainly fine-medium grained, moderately- to well-sorted, bioturbated arkosic sandstones with localised crossbedding and ripples (Kuhn et al., 2003).

At a subsea depth of 3200 m in the Fulmar Field, the Fulmar Formation reservoir has an average formation pressure of 39 MPa (7 MPa above hydrostatic), a vertical effective stress of 31 MPa and a temperature of ~130 °C (Lee and Parsons, 2003; Mehenni and Roodenburg, 1990; Saigal et al., 1992). The overlying Kimmeridge Clay Formation is the main source rock, and also doubles as a seal lithology, jointly with the Upper Cretaceous Chalk in the Fulmar area (Kuhn et al., 2003).

3. Samples and methods

A total of 22 Fulmar Formation sandstone samples from Well 30/16–7 were collected at ~1 m intervals between 3245 and 3277 m TVDSS; all samples were taken from below the oil-water contact.

Optical and electron microscopy-based petrographic analyses were

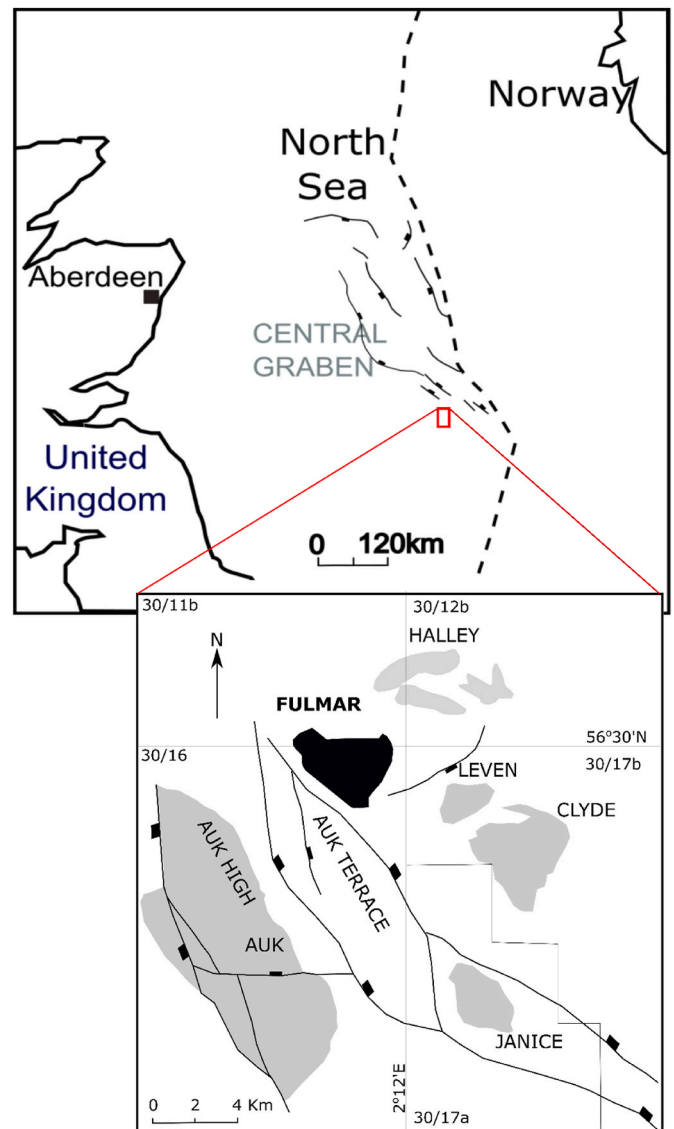


Fig. 1. Map of the study location showing the Fulmar Field and other adjacent fields (adapted from Spaak et al., 1999).

performed on thin sections prepared from the 22 Fulmar Formation samples. During optical microscopy, modal analysis of grain types, grain contacts, grain coats, matrix and cement was carried out by making at least 300 point-counts on each thin section. The results were used to select 10 thin sections representing the full range of quartz cement volumes for further analysis using electron microscopy. Scanning electron microscope cathodoluminescence (SEM-CL) and energy dispersive X-ray (EDX) techniques were used to create both Si element and CL maps of a 9 mm² area of each thin section. These were used to quantify detrital quartz, authigenic quartz and intergranular pressure dissolution (Oye, 2019).

Basin modelling (1D) was performed on PetroMod software (v. 2014.1) to determine the burial, temperature, and effective stress histories of the Fulmar Formation in the Fulmar Field. Stratigraphic layers and their thicknesses were extracted from composite logs (Table 1), and their ages from the Millennium Atlas (Evans et al., 2003). Other data were obtained from an unpublished Operator's report. Heat flow model input parameters were defined using Allen and Allen (2005), with an average of 58 mW/m² and peak heat flows in the Permo-Triassic (69.7 mW/m²) and Upper Jurassic (86.4 mW/m²) representing Central North Sea rifting events. The thermal model was calibrated using measured

Table 1
Layer thicknesses and lithologies used for Fulmar Field burial history modelling (from Oye, 2019).

System	Series	Group	Formation	Age (Ma)	Lithology	Thickness (m)
Paleogene	Eocene - Miocene	Hordaland Group (undiff.)	Nord/Hord	54	Shale (typical)	2687
Paleogene	Eocene	Rogaland	Balder Fm.	56	Shale (silty) 95% Tuff 5%	14
Paleogene	Paleocene	Montrose	Lista Fm.	62.5	Shale 70% Silt 30%	160
Cretaceous		Chalk	Chalk Grp.	91	Chalk 90% Marl 10%	67
Jurassic	Upper	Humber	Kimmeridge C. Fm.	150.7	Shale (8% TOC) 90% Silt 10%	156
Jurassic	Upper	Humber	Kimm/Ribble Sand	151.38	Sandstone (typical)	43
Jurassic	Upper	Humber	Kimm/Avon Shale	152.06	Shale 80% (8% TOC) Silt 20%	29
Jurassic	Upper	Humber	Fulmar Sands	158.4	Sandstone (arkose, quartz rich)	277
Triassic	Lower	Heron	Smith Bank Fm.	248.2	Shale (organic lean, sandy)	142

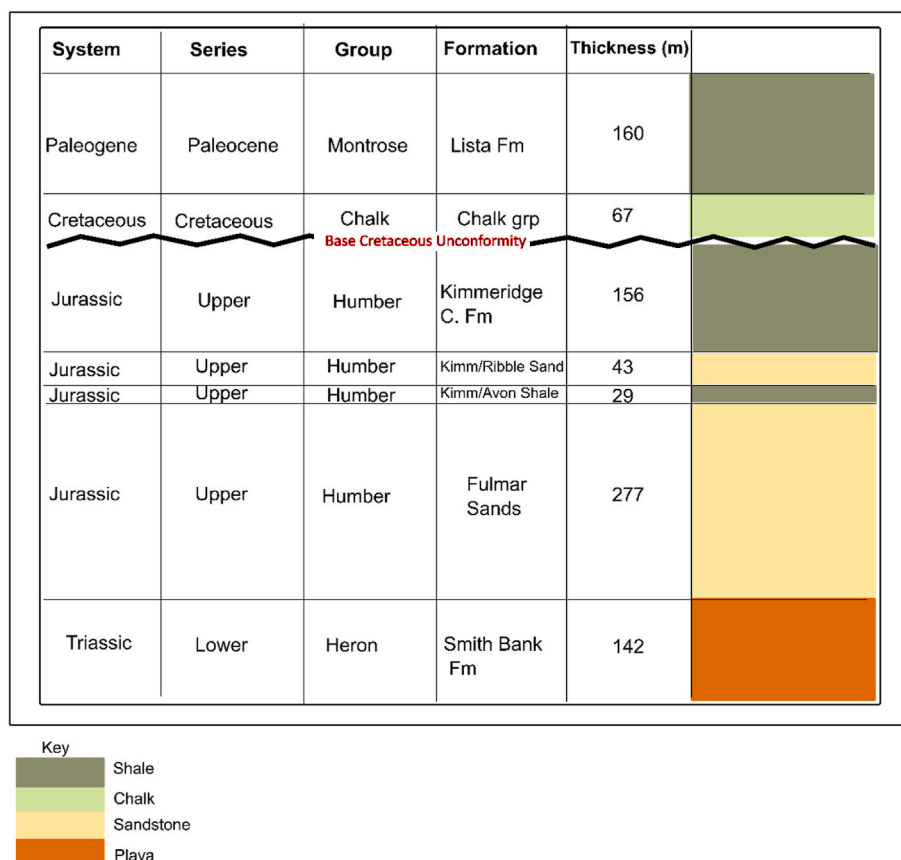


Fig. 2. Stratigraphy of the Fulmar Field from Lista Formation to Smith Bank Formation. Thicknesses are average values estimated from well 30/16–7. Smith Bank Formation is dominated by shale, with isolated sands. Analysed samples were collected from the Fulmar Formation.

temperature and vitrinite reflectance (% R_o) data (see Mehenni and Roodenburg, 1990). Field pore pressure data were used to constrain the VES model and routine core analysis porosity data were used to model compaction. For the modelled pore pressure to match Present-day formation pressures, permeability values of the Chalk Group, Kimmeridge Clay Formation and Heather Formation were modified in PetroMod until an optimum fit was attained (see Swarbrick et al., 2005). In addition, a second VES model was constructed referenced to the proposed timing of a substantial increase in VES inferred from (a) petrographic analysis of intragranular microfractures observed in the studied sandstones and (b) the suggestion by Swarbrick et al. (2005) that pore pressure in the Fulmar Formation sands in the Fulmar-Halley-Clyde region decreased substantially in the last ca. 0.5 Ma due to lateral drainage, resulting in an equivalent increase in effective stress. We return to this important point later. Field pore pressure data were used to constrain the stress model and routine core analysis porosity data were used to model compaction.

A quartz precipitation model was constructed for the Fulmar Field sandstones using the Walderhaug (1996) approach. Model inputs

include grain size, mineralogy, and available quartz surface area which was determined using the mineralogical fraction of detrital quartz and grain coat (clay and microquartz) coverage area estimated from petrographic analysis (Oye et al., 2018; Oye, 2019; Oye et al., 2020). Because the Fulmar sandstones from Fulmar Field have an arkosic composition, only the mineralogical fraction of detrital quartz in the samples were considered in the model.

In situ oxygen isotope ($\delta^{18}O$) analysis was performed on three distinct quartz overgrowths from one thin-section (sample depth is 3293.85 m) using high resolution secondary ion mass spectrometry (SIMS) at the WiscSIMS Lab in the University of Wisconsin. The selected quartz overgrowths range in thickness from 30 to 100 μm , allowing multiple spots for SIMS data acquisition. Before the analysis, the sample was embedded in a polished epoxy mount together with University of Wisconsin quartz standard (UWQ-1) grains (Kita et al., 2009). Profiles of $\delta^{18}O$ were measured across each overgrowth using a 3 μm spot diameter. Detailed results of the SIMS analysis are reported in Table S2 of the supplementary material. A comprehensive description of the analytical

procedures have been detailed elsewhere (Kelly et al., 2007; Kita et al., 2009; Oye et al., 2018; Oye, 2019; Oye et al., 2020; Valley et al., 2009).

4. Results

4.1. Burial, temperature, and effective stress histories

Burial, temperature, and vertical effective stress histories are shown in Fig. 3. Deposition of the sandstone in the Middle Jurassic was followed by approximately 1 km of burial in the Upper Jurassic. There was limited deposition throughout the Cretaceous, after which a second phase of burial continued to the Present-day, with an average burial rate of around 42 m/My. Temperatures were below 70 °C until 60 Ma, before increasing steadily to the present-day temperature of 127 °C (Fig. 3).

Using a 1D modelling approach, it is possible to match the present-day effective stress by manipulating the permeabilities of the chalk and overlying shale-rich units (Fig. 3; Table 1). Model results show a steady increase in effective stress during the main phase of burial from 60 Ma, when the effective stress was around 5 MPa, arriving at the present-day effective stress of 31 MPa (Fig. 3B). However, a study of regional pore pressures in this area strongly suggests that the effective stress history of the Fulmar Formation sands was markedly different as a result of major lateral flow and related rapid pore pressure deflation in

the last ca. 0.5 Ma (Swarbrick et al., 2005). Swarbrick et al. (2005) show that Fulmar Formation sandstones in the Fulmar-Clyde-Halley area have much lower overpressures, around 7 MPa, than sandstones in other pressure compartments buried to similar depths in the same region of the Central North Sea, where overpressures are between 21 and 41 MPa. They also show that channel sands encased within underlying Triassic shales are much more highly overpressured than the Fulmar Formation sands, as are thin turbidite sands in the overlying Jurassic Kimmeridge Clay Formation, the Cretaceous chalk, and the Paleocene sands (Fig. 4). There is an overpressure difference of 18.6 MPa between the Kimmeridge Clay Formation sandstones and the Fulmar Formation sandstones, over a vertical separation of 50 m. Explaining the low overpressures in the Fulmar Formation, combined with much higher overpressures above and below it, requires focussed lateral flow and drainage through the Fulmar Formation to a leak point to the west of the area (Swarbrick et al., 2005). The dewatering of the formations immediately above and beneath the Fulmar Formation is supported by the increased pore pressures observed in both overlying and underlying, isolated sands, with the rate of drainage related to the overall permeability structure of the mudstones which encase them.

The sharpness of the pore pressure changes both above and below the Fulmar Formation (Fig. 4) suggests that depressurisation is a geologically recent phenomenon. Swarbrick et al. (2005) ran several 2D fluid flow models in which lateral leakage and pore pressure reduction was started at 15, 10, 5 and 0.5 Ma, with the best fit to the observed pore pressures occurring in the model in which depressurisation started at

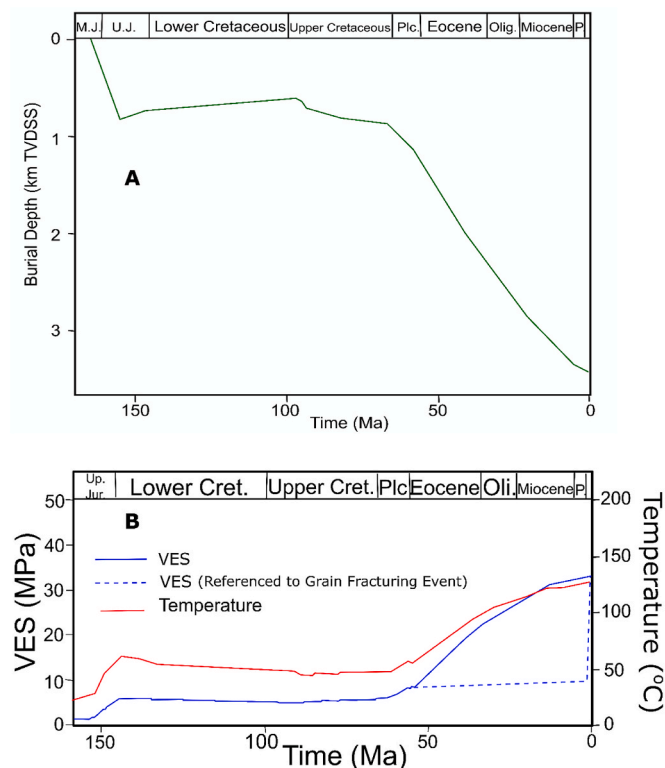


Fig. 3. A) Burial history model for the Fulmar Formation sandstones from Fulmar Field. (M.J – Middle Jurassic, U.J – Upper Jurassic, Plc – Paleocene, Olig. – Oligocene, P. – Pliocene, TVDSS – True vertical depth subsea). B) Modelled temperature and vertical effective stress histories for the Fulmar Formation in the Fulmar Field. Solid blue line is a model in which the permeabilities of mudstones stratigraphically higher than the Fulmar Formation are adjusted to match the present-day pore pressures and effective stress in the Fulmar Formation. Blue dashed line shows the most likely effective stress evolution path based on the paragenesis of the unhealed grain fractures observed in the Fulmar sandstones which validates the suggestion by Swarbrick et al. (2005) that a major decrease in fluid pressure of the Fulmar Formation sandstones occurred in the last ca. 0.5 Ma, (see Fig. 4 and text for further detail). (For interpretation of the references to colour in this figure legend, the reader is referred to the Web version of this article.)

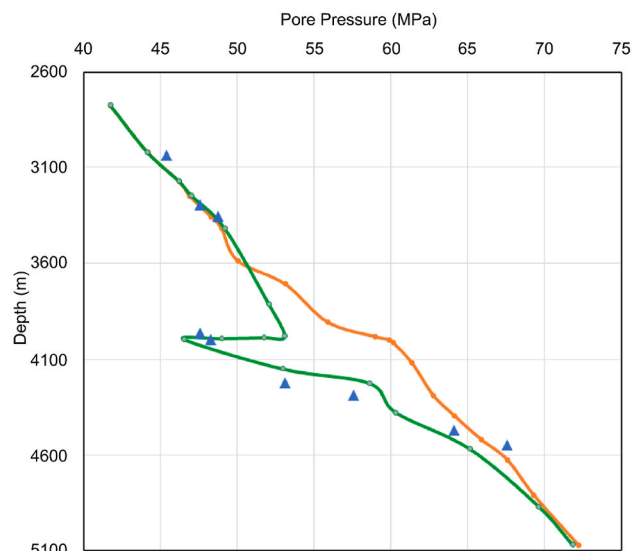


Fig. 4. Pore pressure-depth plot for Well 30/12b-4 in the Halley Field, which is close to the Fulmar Field. Blue triangles are Repeat Formation Test pressure measurements. Similar overpressures also occur in the Fulmar Formation in both the Clyde and Fulmar Fields. The pressure regression is centred on the Fulmar Formation (~4000–4300 m), with more highly overpressured fluids in the overlying Palaeocene and Cretaceous Chalk, and underlying Smith Bank Formation. Orange and green curves are modelled pore pressures from a 2D basin model (Swarbrick et al., 2005). The orange curve represents a scenario in which there is no geologically recent, lateral fluid flow through and out of the Fulmar Formation sands. The green curve is a scenario in which regional depressurisation, centred on the laterally extensive and well-connected Fulmar Formation, started 0.5 Ma ago because of lateral leakage towards the west of the Halley-Clyde-Fulmar-Auk region, probably due to lateral seal failure. Pore pressures show that fluids are also draining into the Fulmar Formation from the underlying Smith Bank Formation, with the rate of drainage dictated by the low permeabilities of the mudstones that dominate that Formation. Figure redrawn from Swarbrick et al. (2005). (For interpretation of the references to colour in this figure legend, the reader is referred to the Web version of this article.)

0.5 Ma (Fig. 4; see Swarbrick et al. (2005) for the full results). The fit is not perfect, which may be expected given uncertainties in both 3D geology and large-scale permeability structures, but the strong implication is that depressurisation occurred very recently in the Fulmar Formation's 160 Ma burial history. The cause of the leakage is not known; Swarbrick et al. (2005) speculate that there was fault seal failure across the basin-bounding fault to the west, towards the North Sea High, perhaps because of repeated ice-loading and unloading.

A model using the same lithological inputs but in which lateral, regional fluid drainage from the Fulmar Formation sands was not allowed, gives a modelled fluid pressure in the Fulmar Formation sands of 60 MPa, compared to the observed 31 MPa (Fig. 4). This implies that prior to pore pressure deflation, the vertical effective stress was on the order of 10 MPa, compared to the actual 31 MPa. For context, in a hydrostatic pressure regime, an effective stress of 10 MPa occurs at around 1 km burial depth.

4.2. Petrographic observations

Fulmar Field sandstones are mainly quartzo-feldspathic with high feldspar content (30%), minor lithic fragments and low clay contents existing either as pore matrix or grain coats (Table 2). These well-sorted, fine-grained sandstones (average size 0.2 mm) have sub-angular to sub-rounded grain shapes. The detrital feldspars are mainly orthoclase (K-feldspar) and minor plagioclase (Na- and Ca-feldspar; Table S1). Some of the feldspars are well preserved, while others are degraded and bear intragranular pores due to dissolution. Feldspar overgrowths were also observed on some of the detrital feldspars. Minor authigenic illitic clay was also observed within intragranular pore spaces of partially dissolved feldspars, replacing the original grains (Fig. 5).

Estimated visible intragranular and intergranular porosities are 0.1 and 18.5% (Table 2). Oversized intergranular pore spaces (~2.8%), which are probably sites of dissolved grains, are also present (Fig. 6). This suggests that intragranular porosity from feldspar dissolution was perhaps underestimated. Helium porosity, taken from an unpublished, internal company report, is up to 30% in Fulmar Field sandstones. This is much more than total visible porosity and could be partly attributed to intragranular micropores that were not captured during modal analysis of petrographic data. Secondly, while quantitative petrographic analysis

Table 2

Summary of petrographic data of the studied Fulmar Formation sandstones from the Fulmar Field. Detailed data are provided in Tables S1 and S2 of the supplementary material.

	No of samples	Mean	Stan. Dev.	Min.	Max.
Detrital grain size (mm)	10	0.2	0.1	0.1	0.5
Quartz (%)	22	40.5	3.2	34.7	46.7
Feldspar (%)	22	30	3.4	23.7	36.7
Lithic Fragments (%)	22	1.2	0.6	0	2.7
Quartz cement - standard petrography (%)	22	2.8	1.7	0	6.3
Quartz cement - CL petrography (%)	10	3.7	2.1	0.9	6.9
Intergranular Pressure Dissolution - CL Petrography (%)	10	1.3	0.6	0.4	2.4
Quartz cement normalised to detrital quartz	10	0.11	0.06	0.03	0.21
Intergranular Pressure Dissolution normalised to detrital quartz	10	0.04	0.02	0.01	0.07
Carbonate cement (%)	22	1	0.5	0	1.7
Intergranular porosity (%)	22	18.5	3.1	14.7	26.7
Intragranular porosity (%)	22	0.1	0.1	0	0.3
Total optical porosity (%)	22	18.6	3.2	13.3	26.7
Core Porosity (%)	23	30	2.7	25.8	35.3
Clay matrix (%)	22	1.4	0.9	0.3	4.3
Intergranular Volume (%)	22	26.1	3	21.7	33.3

was performed using 2D data, helium porosity is measured in 3D. Carbonate is mainly present as pore-occluding cement (Fig. 5), but is scarce and localised within the samples, occurring as less than 1% volume (Table 2).

4.2.1. Grain crushing and fracturing

Qualitative petrographic analysis reveals the presence of microfractures within some of the framework grains (Fig. 7). Features such as corner fracturing, whole-body fracturing, and grain size reduction due to extreme crushing were observed in some of the samples. About 20% of the framework grains are either crushed or fractured. The extent of mineral grain deformation is likely related to their hardness, as most crushed grains are feldspars and most fractured grains are quartz (Fig. 7). The susceptibility of the feldspars to crushing could also be because the grains have been weakened by dissolution. Feldspar dissolution as a product of mid-late diagenesis (Lasocki et al., 1999; Oye et al., 2018) would have initiated long before the recent deflation of pore pressure in the Fulmar Formation. The most striking observation is that the fractures within the quartz grains have not been healed by cement. The occurrence of unhealed fractures within the quartz grains has important implications for the Fulmar Field's vertical effective stress history and will be discussed subsequently.

4.3. Quartz cementation and intergranular pressure dissolution

Blocky macroquartz (commonly called quartz cement) and microcrystalline quartz overgrowths (microquartz) were observed on detrital quartz grains (Fig. 6, Figs. 8 and 9). The microcrystalline quartz overgrowths were observed covering and thus limiting the detrital quartz surface area available for precipitation within intervals between 3294.9 m and 3300.6 m. These intervals are known to host abundant *Rhaxella* sponge spicules (Gowland, 1996).

Optical petrography indicates low volumes of quartz cement (average 2.8%, range 0–6.3%) in the studied samples (Table 2). SEM-CL petrography readily discriminates detrital quartz grains and their overgrowths (Fig. 8), and quartz cement volumes range from 0.9 to 6.9%, with a mean value of 3.7%.

To quantify intergranular pressure dissolution, intergranular boundaries were inspected and projections made on areas with dissolution features in order to restore original grain shapes (Fig. 8) and to estimate, through manual point counting, the volume of material removed by IPD (Oye et al., 2020). This approach is similar to the methods described by Sibley and Blatt (1976) and Houseknecht (1991). The results show that intergranular pressure dissolution released an average of 1.3 volume % of silica (Table 2). This is a substantial part of the silica needed to account for the observed volume of quartz cement, with additional silica supplied from feldspar dissolution.

4.4. Oxygen isotope composition

In situ $\delta^{18}\text{O}$ measurements were made along linear profiles across individual macroquartz overgrowths using high spatial resolution SIMS analysis. Thirty-seven $\delta^{18}\text{O}$ measurements were made on three different overgrowths from one of the Fulmar sandstones. Values of $\delta^{18}\text{O}_{(\text{quartz cement})}$ are plotted as a function of the distance from their detrital grain boundary in Fig. 10. The values show a 3.7‰ range, from +27.9 to +24.2‰. Analysis points that fell on fluid inclusions, cracks or included a mix of detrital and authigenic quartz were discarded. Values of $\delta^{18}\text{O}_{(\text{quartz cement})}$ show a decreasing trend, with heavier values in the earliest-formed cement at the detrital grain-cement boundary, to lighter values in latest-formed cement at the outer edge of the overgrowths (Fig. 10).

4.5. Quartz cementation model

Using the 50% grain-coatings coverage estimated from petrographic

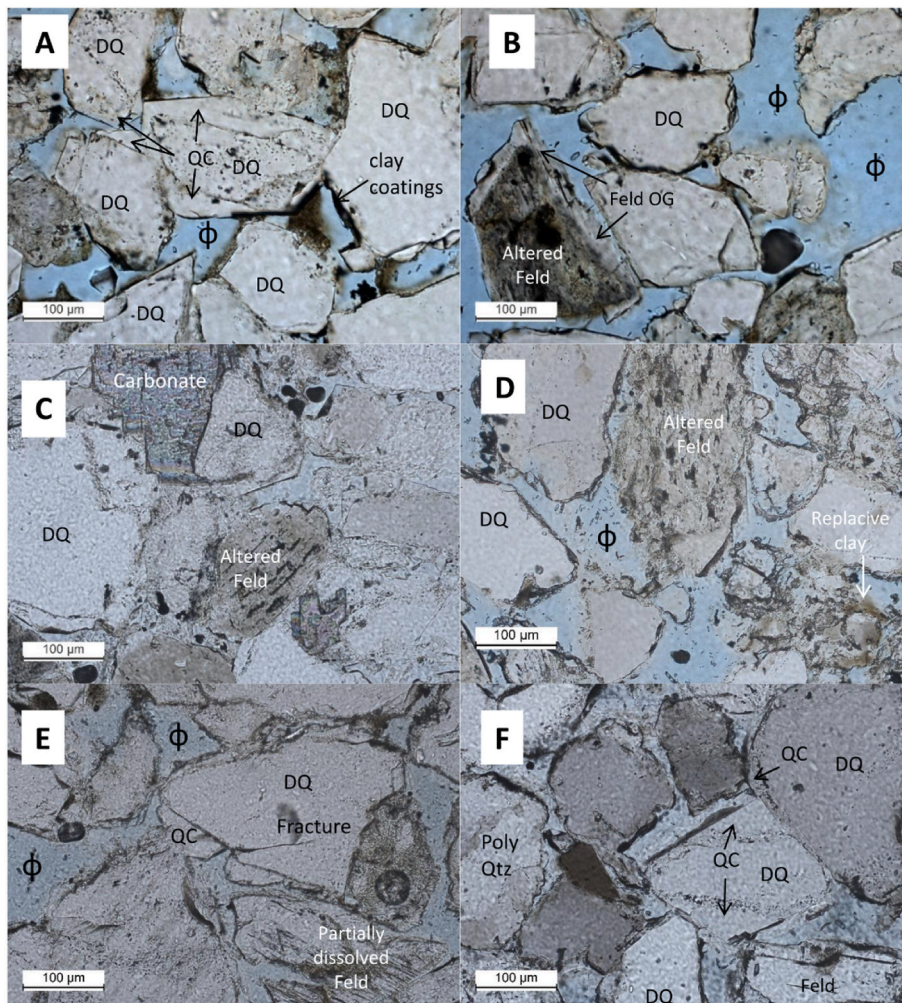


Fig. 5. Optical photomicrographs (plane polarized) of Fulmar Formation sandstones from the Fulmar Field. A) Detrital quartz (DQ) grains with well-developed quartz cement (QC) juxtaposed against those with poorly developed quartz cement due to partial coverage by clay coatings; ϕ is porosity. B) Feldspar grain at the early stage of alteration with a well-developed overgrowth (Feld OG). C) Quartz grains with quartz cement. Slide also shows pore-occluding carbonate cement and partially dissolved feldspar grain with intragranular microporosity. D) Clay (illite?) replacing altered feldspars adjacent to detrital quartz grains with clay coatings. E) Fractured detrital quartz grain with quartz cement and partially dissolved feldspar with intragranular microporosity. The fracture predated significant quartz cement development. F) Detrital quartz, including polycrystalline quartz grains. Quartz cement is more strongly developed on monocrystalline quartz grains.

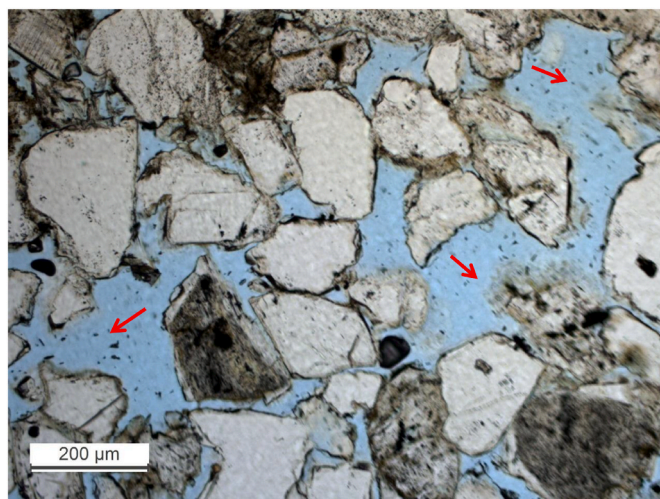


Fig. 6. Oversized pores (red arrows) that are interpreted as sites of completely dissolved feldspars. (For interpretation of the references to colour in this figure legend, the reader is referred to the Web version of this article.)

analyses (Fig. 11), the quartz cementation model (Fig. 12) predicts 7.4% quartz cement volume for the Fulmar sandstones, which is twice the observed volume (3.7%). Half of the cement is predicted to form within the last 15 million years of burial, at temperatures above 120 °C

(Fig. 3B).

5. Pore pressure deflation and grain fracturing

A key observation in this study is that unhealed, intragranular microfractures are common within framework grains, despite a burial temperature of about 130 °C. Here, we consider the implications of this observation for pore pressure and vertical effective stress histories in the Fulmar Formation sandstones.

Framework grain crushing and fracturing is observed in approximately 20% of grains in samples retrieved from certain intervals (e.g. 3296–3297 m MD), similar to those observed by Chuhan et al. (2003, 2002) in sands compacted experimentally to 20–30 MPa effective stress. With the caveat that experimental strain rates are many orders of magnitude higher than geological rates, Chuhan et al. (2003, 2002) indicated only minor grain fracturing below 10 MPa effective stress, with increased fracturing with increasing stress. We propose that rapid pore pressure reduction led to a sharp rise in vertical effective stress, and that the geologically rapid stress increase led to the fracturing of the framework grains. Grain crushing and fracturing occurred because the sandstones were (and are) poorly cemented, resulting in low compressive strength. Similar observations have been made in deeply-buried sandstones in the Haltenbanken area, in which quartz cementation was inhibited by extensive chlorite grain coatings (Chuhan et al., 2002). In that case, fractures within quartz grains had been healed by quartz cement, and it is well-known that newly created fracture surfaces provide kinetically favourable sites for quartz precipitation (e.g. Fisher

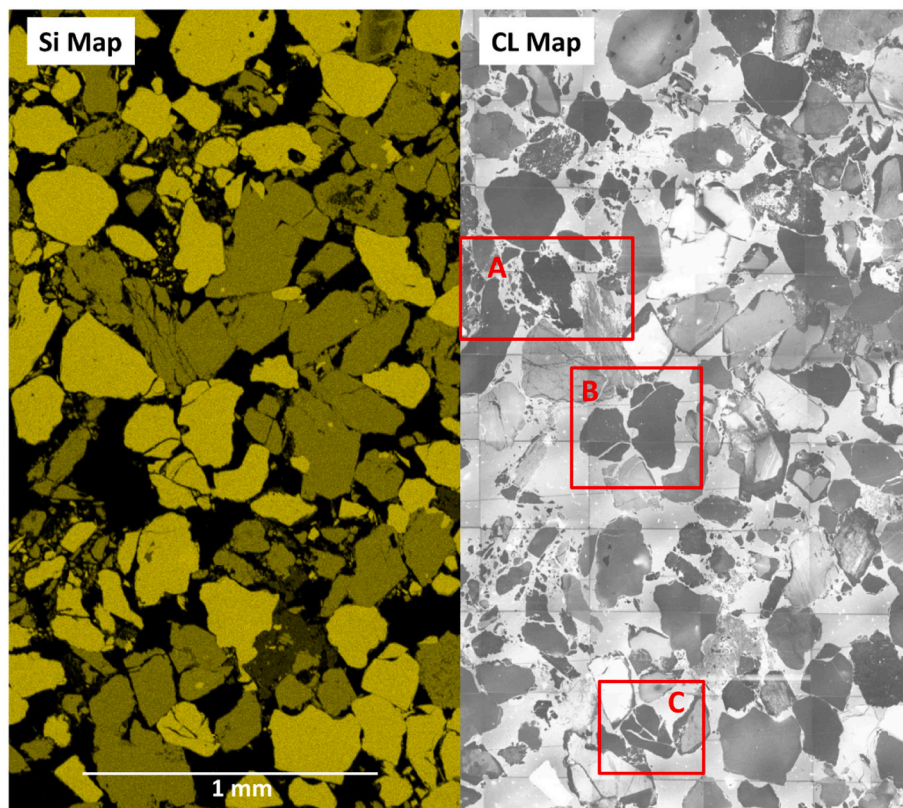


Fig. 7. Silica (Si) map from EDX analysis (left) and montaged SEM-CL map (right) showing crushed and fractured framework grains. Fracturing was likely due to recent rapid depressuring of the Fulmar Formation in the last 0.5 Ma. On the silica map, bright yellow grains represent quartz; feldspar is dull yellow-green. Slides A, B and C are zoomed copies of the insets on the CL montage. A) shows crushed framework grains (feldspars) and their finer products; B) shows corner fracturing of framework grains (quartz), and C) shows whole body fracturing of framework grains (quartz). Note that the fractures are unhealed (open). (For interpretation of the references to colour in this figure legend, the reader is referred to the Web version of this article.)

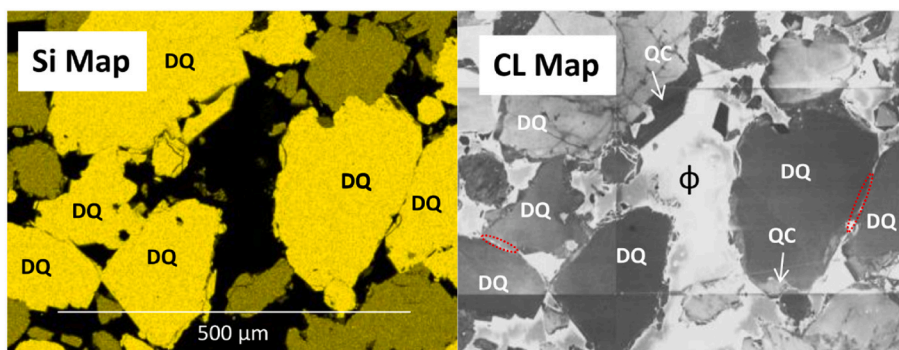
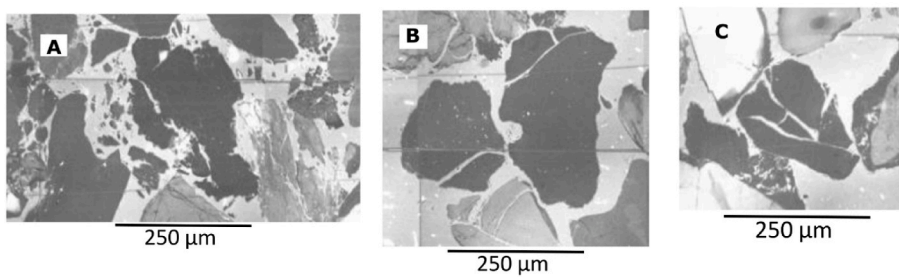


Fig. 8. Silica map generated from EDX analysis (left) and equivalent montaged cathodoluminescence (CL) map (right) of Fulmar Formation sandstones showing detrital quartz (DQ), quartz cement (QC), and some projected grain boundaries representing chemical compaction features. Bright yellow grains on the silica map represent quartz; feldspar grains are dull yellow-green. ϕ is porosity. (For interpretation of the references to colour in this figure legend, the reader is referred to the Web version of this article.)

et al., 1999). Since the kinetics of quartz cementation in fractures is suggested to be faster ($>2 \mu\text{m}/\text{m.y.}$) than that of the host rock (Lander and Laubach, 2015), the presence of quartz grains with unhealed fractures in the current study strongly indicate a geologically recent depressurisation and fracturing event. These results are consistent with the suggestion made by Swarbrick et al. (2005), based on trends observed in regional pressure data (Fig. 4), that the currently low pore pressure and high effective stress in the studied Fulmar Formation only

developed in the last ca. 0.5 Ma.

These results suggest that vertical effective stress was below 10 MPa through almost the entire burial history of the Fulmar Formation in the Fulmar Field, only increasing to 31 MPa in the last 0.5 My (Fig. 3B). Whilst we still require a sufficiently accurate and robust model relating the rate of IPD to VES (see van Noort et al., 2008), the very limited IPD (1.3 vol %) observed here is qualitatively consistent with a low VES history.

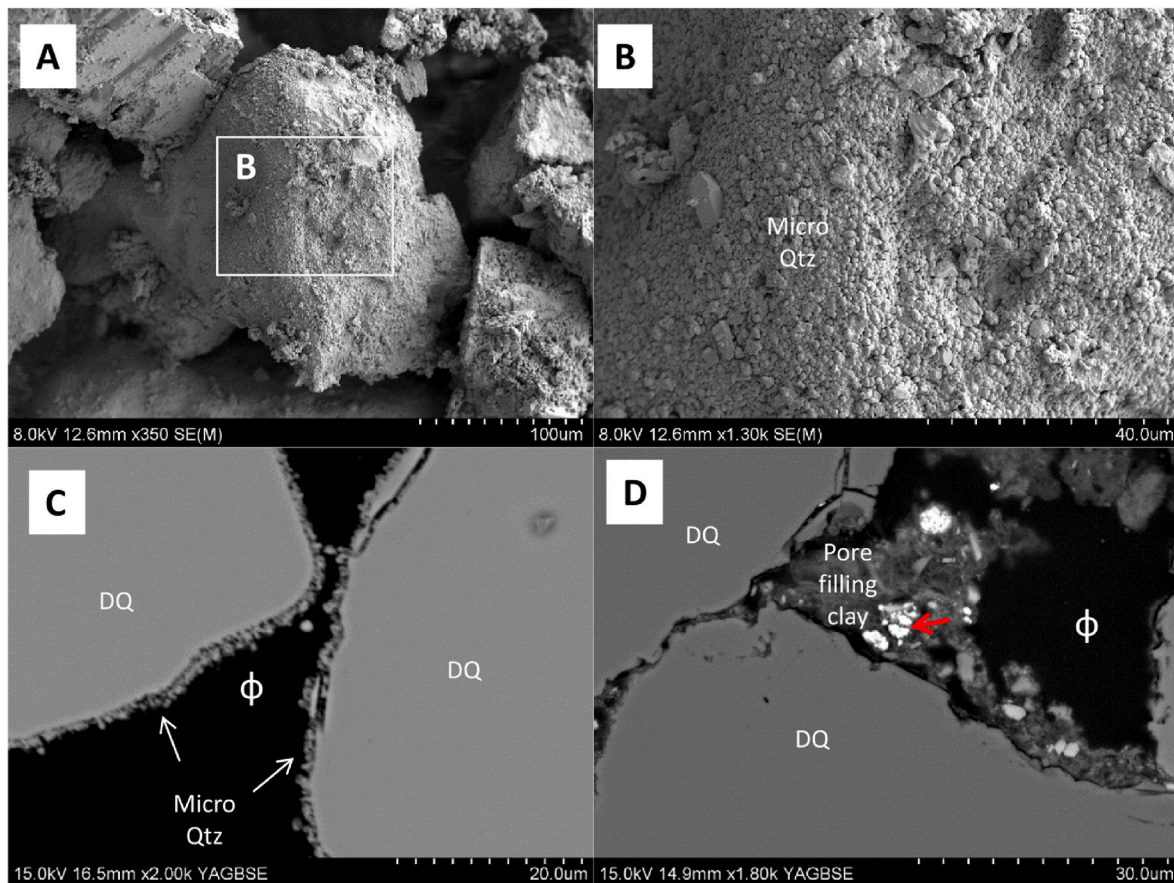


Fig. 9. Electron micrographs of Fulmar Formation sandstones from Fulmar Field. A) Secondary electron image of microquartz overgrowth nucleated on detrital quartz (DQ). B) Higher magnification view equivalent to the box in panel A (image from Fig. 3.15 C in Oye (2019)); C) Backscattered electron (BSE) image showing microquartz overgrowth on detrital quartz grain; D) BSE image showing pore-filling clay mixed with sparse pyrite (red arrow), juxtaposed against detrital quartz. ϕ is porosity. (For interpretation of the references to colour in this figure legend, the reader is referred to the Web version of this article.)

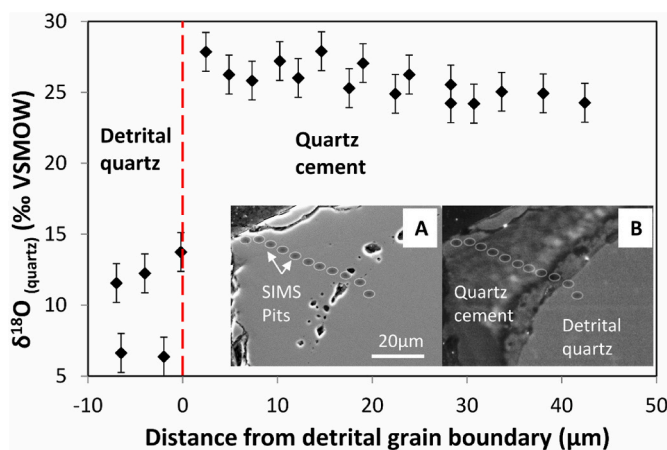


Fig. 10. $\delta^{18}O$ of quartz cement and detrital quartz plotted against lateral distance from detrital grain boundary. Data are from three quartz overgrowths from the same thin section. $\delta^{18}O$ line profile across one of the analysed overgrowths, created using 3 μm diameter sampling spots (SIMS pits), is shown in Insets A and B (BSE and CL micrographs).

5.1. Implications for quartz cementation

Vertical effective stress (VES) is the primary control on the rate of intergranular pressure dissolution (IPD) along grain–grain contacts, with a secondary control by temperature (Elias and Hajash, 1992; Nenna

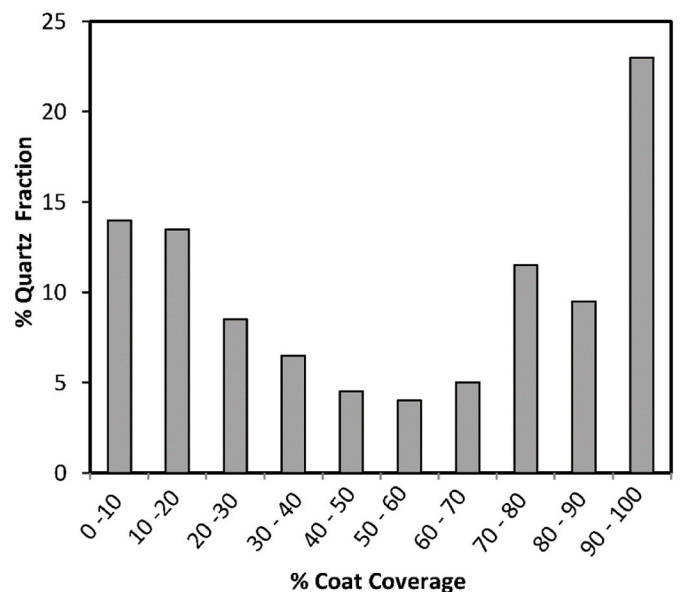


Fig. 11. Histogram showing percentage grain coat coverage (clays and microquartz) of detrital quartz grains. The average grain coat coverage is approximately 50%, although the data are bimodal.

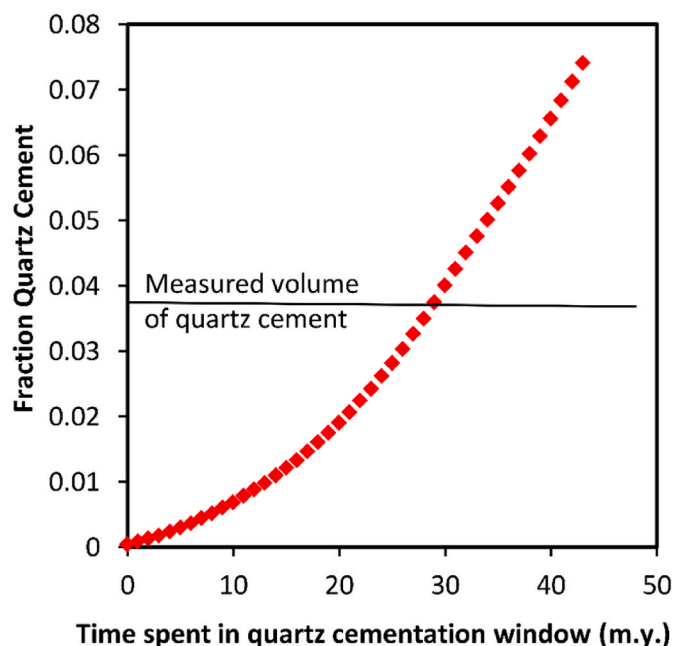


Fig. 12. Kinetic model of quartz cementation constructed for the Fulmar Formation from Fulmar Field based on the Walderhaug (1996) approach. A precipitation threshold temperature of 80 °C and an average grain coating (clays and microquartz) coverage of 50% were applied in the model.

and Aydin, 2011; Oye et al., 2018, 2020; Sheldon et al., 2003; van Noort et al., 2008). Should the supply of silica via IPD be the rate-limiting step for quartz cementation, one would expect to observe relationships between cement volumes and (a) volumes of quartz released by IPD and (b) effective stress histories. Relatively few datasets have tested these relationships because firstly, quantitative, statistically robust data for IPD are difficult to obtain using optical petrography and is time-consuming to acquire using SEM-CL; and secondly, accurate pore pressure and effective stress histories are much more difficult to determine than temperature histories, requiring robust models with detailed geological inputs and for which there is very little calibration except for the present-day pore pressure. As illustrated by the present study, present-day pore pressures and effective stresses are not necessarily accurate guides to past pore pressures, so that observations of low volumes of quartz cement in currently high effective stress sandstones does not prove that VES history is not a control on silica supply (IPD) and cementation rate (Bjorkum and Nadeau, 1998; Walderhaug, 1994a, 1994b).

In this study, the oxygen isotope data, quartz cement volume and cementation history are consistent with a model in which the rate-limiting step in the cementation process is silica supply from intergranular pressure dissolution rather than temperature-related precipitation kinetics or transport of aqueous silica.

The interpretation framework for the oxygen isotopic composition of quartz cement in these sandstones is shown in Fig. 13. The $\delta^{18}\text{O}$ value of the earliest-formed quartz cement is +27.9‰. If precipitation started in water with $\delta^{18}\text{O}_{(\text{water})}$ of -1‰, similar to the Jurassic seawater in which the Fulmar Formation was deposited, this corresponds to a temperature of 50 °C, which is below the commonly recognised 70–80 °C threshold for quartz cement (Walderhaug, 1994a, 1996). If cementation started at 80 °C, the water would have an isotopic composition of around 4‰, which is the same as the current water in the Fulmar Formation (+4.2‰; Macaulay et al., 1997). For the lowest $\delta^{18}\text{O}_{(\text{quartz cement})}$ of +24.2‰, precipitation from current Fulmar Formation water would then occur at 110 °C (Fig. 10), compared to the present-day temperature of 127 °C. Although we did not measure the isotopic composition of the outermost few microns of the cement, these results strongly suggest that very little

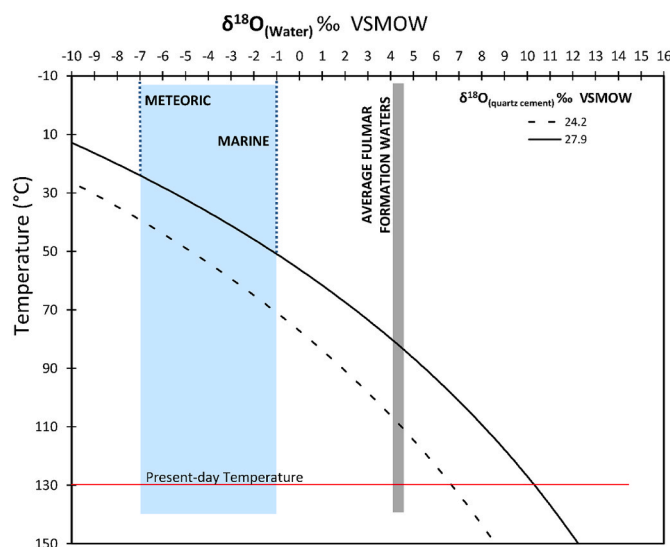


Fig. 13. Plot of $\delta^{18}\text{O}_{\text{water}}$ in equilibrium with $\delta^{18}\text{O}_{(\text{quartz cement})}$ of +27.9‰ and +22.4‰, the extreme values measured in this study, as a function of temperature for the Fulmar Formation from Fulmar Field (fractionation factors from Matsuhisa et al. (1979)). Grey bar indicates the current $\delta^{18}\text{O}_{\text{water}}$ in the Fulmar Formation. $\delta^{18}\text{O}_{\text{water}}$ likely evolved from Jurassic marine water to present-day formation water (4.2‰).

cementation occurred above ca. 110 °C, and so over the last 25 Ma (Fig. 3B). This is contrary to the predictions of the temperature-controlled cementation model, in which 80% of the predicted 7.4% cement would have formed in the last 25 Ma, between 110 and 127 °C (Fig. 12). Quartz cement may have precipitated to maximum temperature, but the volumes of any late-formed quartz are small, suggesting a very low rate of precipitation.

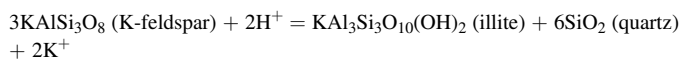
Whilst low volumes of quartz cement partly reflect the reduction of available quartz surface area due to grain-coating microquartz and clay (Aase et al., 1996; French et al., 2021), this alone cannot explain the low cement volumes. The combined average grain-coat coverage of clay and microquartz in the studied samples is around 50% (Fig. 11) and is the value which we used in the temperature-based precipitation model to reduce the surface area available for quartz crystal growth. However, the volumes of quartz cement predicted from the temperature-controlled precipitation kinetic model (7.4%) are, on average, twice those observed petrographically (3.7%), including samples that contain limited or no microquartz. Model runs using different coating coverage show that a grain-coat coverage of 80% on individual detrital grains is required to account for the average observed quartz cement value of 3.7%. Only 30% of grains have >80% coatings, with around half having less than 50% (Fig. 11).

In terms of transport, many previous studies support the idea that deep-burial sandstone diagenesis can be considered as a rock-dominated, semi-closed system in which only diffusive and/or local advective transport is required to account for the observed mineralogical and chemical changes (Bjørlykke, 2014; Taylor et al., 2010); transport is not considered to be rate-limiting, except perhaps in hydrocarbon reservoirs where the rate of diffusion or advection may be slowed by the replacement of pore water with hydrocarbons (Taylor et al., 2010; Worden et al., 2018). This, however, is not relevant here because the samples were taken from below the oil-water contact in a well drilled on the flank of the structure, in a sandstone unit for which there is no strong evidence for the occurrence of a deeper palaeo-oil column (Saigal et al., 1992; Kuhn et al., 2003).

Since IPD only supplies one third of the silica observed as quartz cement, a second source is required, which we suggest is from the dissolution of potassium feldspars. Feldspar dissolution in Fulmar Formation sands is widespread (Wilkinson et al., 1997; Wilkinson and

Haszeldine, 1996), increasing with temperature, and is commonly observed in arkosic sandstones at temperatures in excess of 100 °C (Bjørlykke et al., 1995; Milliken et al., 1989; Yuan et al., 2015). In these samples feldspar dissolution is observed as grains that have been partly replaced by illitic clays and is also inferred from the occurrence of ~2.8% oversized pores which were once feldspar grains (Fig. 6). The occurrence of oversized pores implies that dissolution and alteration of feldspar grains occurred when already deeply buried, as early dissolution would have resulted in pore collapse by mechanical compaction. The reaction of potassium feldspar to give the more thermodynamically stable assemblage of illite and quartz is a common diagenetic reaction in both sandstones and mudstones (in which smectite is also involved) and can proceed without the requirement for external reactants, such as a source of acid (e.g. Giles and De Boer, 1990). The reactions are kinetically controlled and increase with temperature above ca. 100 °C (see Yuan et al., 2019 for a review). In Fulmar Formation sands from the Central North Sea, potassium feldspar is increasingly and extensively lost at depths between 3000 m and 4500 m (Wilkinson and Haszeldine, 1996), so that the samples in this study are in the early part of that process.

A balanced reaction for the transformation of K feldspar to illite and quartz is:



Assuming that the oversized pores are the result of feldspar dissolution, then the combined volume of intragranular porosity and oversized pores (~2.9%) would also result in 4.8% quartz and 1% illite. The volume of illite estimated is close to the 1.4% quantified from petrographic analysis, suggesting that most of the illite in these high energy, shoreface sands are formed diagenetically from feldspar dissolution. Most importantly, it is reasonable to suggest that feldspar dissolution can supply the 2.4% silica required for the observed 3.7% quartz cement, above the 1.3% that can be supplied from IPD. The mass balance suggests that it is possible that silica has been exported from the frame of reference of this study, perhaps due to the geologically recent fluid flow through the Fulmar Formation, indicated by the observed pore pressure distribution (Swarbrick et al., 2005).

Given the potential complexities of effective stress and pore pressure histories, simple relationships between current effective stress and quartz cement volumes are unlikely to occur. Key implications of this study are that (1) information from palaeo-stress indicators like grain fractures can help place tighter constraints on effective stress history models and (2) an accurate vertical effective stress history should be considered as part of any predictive model of quartz cementation in sandstones.

6. Conclusions

Upper Jurassic Fulmar Formation sandstones from the Fulmar Field in the Central North Sea contain very limited quartz cement, substantially less than would be predicted by commonly used models based on temperature-related quartz precipitation kinetics. Oxygen isotope microanalysis of three well-developed quartz overgrowths within the studied sandstones suggests that only limited cementation occurred at temperatures between ca. 110 °C and the present-day temperature of 128 °C. Intergranular pressure dissolution accounts for around one third of the observed quartz cement, with the remaining quartz cement accounted for by deep-burial feldspar dissolution. Hydrocarbon charge cannot account for the low quartz cement contents as the sandstones occur in non-hydrocarbon-bearing intervals.

Because the sands are at a high effective stress at the present-day, there is no obvious reason to support a view that the low volumes of quartz cement reflect a lack of supply of silica from stress-controlled intergranular pressure dissolution. However, we suggest that the

anomalously low volumes of quartz cement are in fact most readily explained by the unusual pore pressure and effective stress histories of the Fulmar Formation in this region. Swarbrick et al.'s (2005) regional pore pressure analysis implies that the regional Fulmar Formation was depressurised in the last <0.5 Ma, increasing effective stress from ca. 10 MPa to the current 31 MPa. A geologically recent increase in effective stress is supported by the common occurrence of fractured grains in detrital quartz grains, and the fact that the fractures remain unhealed by quartz. We argue that a continuous history of low effective stress, until the very recent geological past, limited the rate of intergranular pressure dissolution and silica supply, and by extension, the rate of quartz cementation.

These results also demonstrate how petrographic data can help to constrain effective stress histories and may provide information about inflection points in effective stress evolution. Future predictive models for reconstructing how reservoir sandstones become quartz cemented during burial diagenesis should incorporate well-constrained effective stress histories.

Credit author statement

Olakunle Oye: Methodology, Investigation, Writing – original draft, Visualisation, Funding acquisition. Andrew Aplin: Conceptualization, Resources, Writing – review & editing, Supervision, Funding acquisition. John Valley: Writing – review & editing, Funding acquisition. Ian Orland: Supervision, Writing – review & editing

Declaration of competing interest

The authors declare that they have no known competing financial interests or personal relationships that could have appeared to influence the work reported in this paper.

Data availability

Data are in manuscript and/or are in Supplementary Material

Acknowledgements

Petroleum Technology Development Fund, Nigeria is thanked for funding this research. We acknowledge support from the British Geological Survey (BGS) for access to core material, and Information Handling Services (IHS) for access to data from Fulmar Field well. WiscSIMS is supported by NSF (EAR-1658823, 2004618) and UW-Madison. Thanks to two anonymous reviewers for their very constructive comments on the manuscript.

Appendix A. Supplementary data

Supplementary data to this article can be found online at <https://doi.org/10.1016/j.geoen.2022.211383>.

References

- Aase, N.E., Bjørkum, P.A., Nadeau, P.H., 1996. The effect of grain-coating microquartz on preservation of reservoir porosity. *AAPG Bull.* 80, 1654–1673. <https://doi.org/10.1306/64eda0f0-1724-11d7-8645000102c1865d>.
- Allen, P.A., Allen, J.R., 2005. *Basin Analysis: Principles and Applications*. Wiley-Blackwell, p. 549.
- Bjorkum, P.A., Nadeau, P.H., 1998. Temperature controlled porosity/permeability reduction, fluid migration, and petroleum exploration in sedimentary basins. *The APPEA Journal* 38, 453–465.
- Bjørlykke, K., 2014. Relationships between depositional environments, burial history and rock properties. Some principal aspects of diagenetic process in sedimentary basins. *Sediment. Geol.* 301, 1–14. <https://doi.org/10.1016/j.sedgeo.2013.12.002>.
- Bjørlykke, K., Aagaard, P., Egeberg, P.K., Simmons, S.P., 1995. *Geochemical constraints from formation water analyses from the North Sea and the Gulf Coast Basins on quartz, feldspar and illite precipitation in reservoir rocks*. Geological Society, London, Special Publication 86, 33–50.

- Chuhan, F.A., Kjeldstad, A., Bjørlykke, K., Høeg, K., 2002. Porosity loss in sand by grain crushing—experimental evidence and relevance to reservoir quality. *Mar. Petrol. Geol.* 19, 39–53.
- Chuhan, F.A., Kjeldstad, A., Bjørlykke, K., Høeg, K., 2003. Experimental compression of loose sands: relevance to porosity reduction during burial in sedimentary basins. *Can. Geotech. J.* 40, 995–1011. <https://doi.org/10.1139/t03-050>.
- DiGiovanni, A., Fredrich, J., Holcomb, D., Olsson, W., 2007. Microscale damage evolution in compacting sandstone. Geological Society, London, Special Publication 289, 89–103.
- Elias, B.P., Hajash, A., 1992. Changes in quartz solubility and porosity due to effective stress: an experimental investigation of pressure solution. *Geology* 20, 451–454. [https://doi.org/10.1130/0091-7613\(1992\)020<0451:CIQSAP>2.3.CO](https://doi.org/10.1130/0091-7613(1992)020<0451:CIQSAP>2.3.CO).
- Evans, D., Graham, C., Armour, A., Bathurst, P., 2003. In: *The Millennium Atlas: Petroleum Geology of the Central and Northern North Sea*. Geological Society of London, London, Bath, p. 389.
- Fisher, Q.J., Casey, M., Clennell, M.B., Knipe, R.J., 1999. Mechanical compaction of deeply buried sandstones of the North Sea. *Mar. Petrol. Geol.* 16, 605–618.
- French, M.W., Worden, R.H., King, H.E., Horn, W.C., Lamberti, W.A., Shosa, J.D., 2021. The origin of silica cements revealed by spatially resolved oxygen isotope microanalysis and electron-beam microscopy; Heidelberg Formation, Germany. *Geochim. Cosmochim. Acta* 309, 57–78. <https://doi.org/10.1016/j.gca.2021.06.019>.
- Giles, M.R., De Boer, R.B., 1990. Origin and significance of redistributional secondary porosity. *Mar. Petrol. Geol.* 7, 378–397.
- Govland, S., 1996. Facies characteristics and depositional models of highly bioturbated shallow marine siliciclastic strata: an example from the Fulmar Formation (Late Jurassic), UK Central Graben. Geological Society, London, Special Publications 114, 185–214.
- Houseknecht, D.W., 1991. Use of Cathodoluminescence Petrography for Understanding Compaction, Quartz Cementation, and Porosity in Sandstones. SEPM Special Publication. SC25, 59–66.
- Kelly, J.L., Fu, B., Kita, N.T., Valley, J.W., 2007. Optically continuous silcrete quartz cements of the St. Peter Sandstone: high precision oxygen isotope analysis by ion microprobe. *Geochim. Cosmochim. Acta* 71, 3812–3832. <https://doi.org/10.1016/j.gca.2007.05.014>.
- Kita, N.T., Ushikubo, T., Fu, B., Valley, J.W., 2009. High precision SIMS oxygen isotope analysis and the effect of sample topography. *Chem. Geol.* 264, 43–57. <https://doi.org/10.1016/j.chemgeo.2009.02.012>.
- Kuhn, O., Smith, S.W., Van Noort, K., Loiseau, B., 2003. The fulmar field, Blocks 30/16, 30/11b, UK North Sea. Geological Society Memoir 20, 563–585. <https://doi.org/10.1144/GSL.MEM.2003.020.01.46>.
- Lander, R.H., Laubach, S.E., 2015. Insights into rates of fracture growth and sealing from a model for quartz cementation in fractured sandstones. *AAPG Bull.* 127, 516–538.
- Lander, R.H., Walderhaug, O., 1999. Predicting porosity through simulating sandstone compaction and quartz cementation. *AAPG Bull.* 83, 433–449. <https://doi.org/10.1306/00aa9bc4-1730-11d7-8645000102c1865d>.
- Lasocki, J., Guemene, J., Hedayati, A., Legorjus, C., Page, W., 1999. The Elgin and Franklin fields: UK Blocks 22/30c, 22/30b and 29/5b. In: *Geological Society, London, Petroleum Geology Conference Series*. Geological Society of London, pp. 1007–1020.
- Laubach, S.E., 1989. Paleostress directions from the preferred orientation of closed microfractures (fluid-inclusion planes) in sandstone, East Texas basin, USA. *J. Struct. Geol.* 11, 603–611.
- Lee, M.R., Parsons, I., 2003. Microtextures of authigenic or-rich feldspar in the upper jurassic humber Group, UK North Sea. *Sedimentology* 50, 597–608. <https://doi.org/10.1046/j.1365-3091.2003.00567.x>.
- Macaulay, C.I., Boyce, A.J., Fallick, A.E., Haszeldine, R.S., 1997. Quartz veins record vertical flow at a Graben edge: Fulmar oil field, central North Sea. *AAPG (Am. Assoc. Pet. Geol.) Bull.* 81, 2024–2035. <https://doi.org/10.1306/3b05c712-172a-11d7-8645000102c1865d>.
- Makowitz, A., Milliken, K.L., 2003. Quantification of brittle deformation in burial compaction, Frio and Mount Simon Formation sandstones. *J. Sediment. Res.* 73, 1007–1021.
- Matsuhisa, Y., Goldsmith, J.R., Clayton, R.N., 1979. Oxygen isotopic fractionation in the system quartz-albite-anorthite-water. *Geochim. Cosmochim. Acta* 43, 1131–1140.
- McBride, E.F., 1989. Quartz cement in sandstones: a review. *Earth Sci. Rev.* 26, 69–112. [https://doi.org/10.1016/0012-8252\(89\)90019-6](https://doi.org/10.1016/0012-8252(89)90019-6).
- Mehenni, M., Roodenburg, W.Y., 1990. Fulmar Field - UK south central graben, North Sea. In: Foster, N.H., Beaumont, E.A. (Eds.), *Structural Traps IV: Tectonic and Nontectonic Fold Traps*, AAPG Treatise of Petroleum Geology/Atlas of Oil and Gas Fields, pp. 113–139.
- Milliken, K.L., McBride, E.F., Land, L.S., 1989. Numerical assessment of dissolution versus replacement in the subsurface destruction of detrital feldspars, Oligocene Frio Formation, South Texas. *J. Sediment. Res.* 59, 740–757.
- Nenna, F., Aydın, A., 2011. The formation and growth of pressure solution seams in clastic rocks: a field and analytical study. *J. Struct. Geol.* 33, 633–643. <https://doi.org/10.1016/j.jsg.2011.01.014>.
- Osborne, M.J., Swarbrick, R.E., 1997. Mechanisms for generating overpressure in sedimentary basins: a reevaluation. *AAPG Bull.* 81, 1023–1041.
- Oye, O.J., 2019. Influence of fluid pressure and effective stress on quartz cementation in clastic reservoirs. Ph.D thesis, Durham University.
- Oye, O.J., Aplin, A.C., Jones, S.J., Gluyas, J.G., Bowen, L., Harwood, J., Orland, I.J., Valley, J.W., 2020. Vertical effective stress and temperature as controls of quartz cementation in sandstones: evidence from North Sea Fulmar and Gulf of Mexico Wilcox sandstones. *Mar. Petrol. Geol.* 115, 104289. <https://doi.org/10.1016/j.marpetgeo.2020.104289>.
- Oye, O.J., Aplin, A.C., Jones, S.J., Gluyas, J.G., Bowen, L., Orland, I.J., Valley, J.W., 2018. Vertical effective stress as a control on quartz cementation in sandstones. *Mar. Petrol. Geol.* 98, 640–652. <https://doi.org/10.1016/j.marpetgeo.2018.09.017>.
- Pijnenburg, R.P.J., Verberne, B.A., Hangx, S.J.T., Spiers, C.J., 2019. Inelastic Deformation of the Slochteren Sandstone: Stress-Strain Relations and Implications for Induced Seismicity in the Groningen Gas Field. *Journal of Geophysical Research: Solid Earth*. <https://doi.org/10.1029/2019JB017366>.
- Saigal, G.C., Bjørlykke, K., Larter, S., 1992. The effects of oil emplacement on diagenetic processes—examples from the Fulmar reservoir sandstones, Central North Sea. *AAPG Bull.* 76, 1024–1033. <https://doi.org/10.1306/BDF8966-1718-11D7-8645000102C1865D>.
- Sheldon, H.A., Wheeler, J., Worden, R.H., Cheadle, M.J., 2003. An analysis of the roles of stress, temperature, and pH in chemical compaction of sandstones. *J. Sediment. Res.* 73, 64–71. <https://doi.org/10.1306/070802730064>.
- Sibley, D.F., Blatt, H., 1976. Intergranular pressure solution and cementation of the Tuscarora orthoquartzite. *J. Sediment. Res.* 46, 881–896.
- Spaak, P., Almond, J., Salahudin, S., Mohd Salleh, Z., Tosun, O., 1999. Fulmar: a mature field revisited. Geological Society, London, Petroleum Geology Conference Proceedings 5, 1089–1100. <https://doi.org/10.1144/0051089>.
- Swarbrick, R.E., Seldon, B., Mallon, A.J., 2005. In: *Modelling the Central North Sea pressure history*. Geological Society London, pp. 1237–1245.
- Taylor, T.R., Giles, M.R., Hathon, L.A., Diggs, T.N., Braunsdorf, N.R., Birbiglia, G.V., Kittridge, M.G., MacAulay, C.I., Espejo, I.S., 2010. Sandstone diagenesis and reservoir quality prediction: models, myths, and reality. *AAPG Bull.* 94, 1093–1132. <https://doi.org/10.1306/04211009123>.
- Teufel, L.W., Rhett, D.W., Farrell, H.E., 1991. Effect of reservoir depletion and pore pressure drawdown on in situ stress and deformation in the Ekofisk field, North Sea. 32nd U.S. Symposium on Rock Mechanics, USRMS 1991, pp. 63–72.
- Valley, J.W., Kita, N.T., Fayek, M., 2009. In situ oxygen isotope geochemistry by ion microprobe. *MAC Short Course: Secondary Ion Mass Spectrometry in the Earth Sciences* 41, 19–63.
- van Noort, R., Spiers, C.J., Pennock, G.M., 2008. Compaction of granular quartz under hydrothermal conditions: controlling mechanisms and grain boundary processes. *J. Geophys. Res. Solid Earth* 113, 1–23. <https://doi.org/10.1029/2008JB005815>.
- Verberne, B.A., Hangx, S.J.T., Pijnenburg, R.P.J., Hamers, M.F., Drury, M.R., Spiers, C.J., 2021. Drill core from seismically active sandstone gas reservoir yields clues to internal deformation mechanisms. *Geology* 49, 483–487. <https://doi.org/10.1306/G48243.1>.
- Walderhaug, O., 1996. Kinetic modeling of quartz cementation and porosity loss in deeply buried sandstone reservoirs. *AAPG Bull.* 80, 731–745.
- Walderhaug, O., 1994a. Temperatures of quartz cementation in Jurassic sandstones from the Norwegian continental shelf - evidence from fluid inclusions. *J. Sediment. Res.: Sedimentary Petrology & Processes* 64, 311–323. <https://doi.org/10.1306/d4267d89-2b26-11d7-8648000102c1865d>.
- Walderhaug, O., 1994b. Precipitation rates for quartz cement in sandstones determined by fluid-inclusion microthermometry and temperature-history modeling. *J. Sediment. Res.: Sedimentary Petrology & Processes* 64, 324–333. <https://doi.org/10.2110/jsr.64.324>.
- Wilkinson, M., Darby, D., Haszeldine, R.S., Couples, G.D., 1997. Secondary porosity generation during deep burial associated with overpressure leak-off: Fulmar formation, United Kingdom Central Graben. *AAPG Bull.* 81, 803–813. <https://doi.org/10.1306/522b484d-1727-11d7-8645000102c1865d>.
- Wilkinson, M., Haszeldine, R.S., 1996. Aluminium loss during sandstone diagenesis. *J. Geol. Soc.* 153, 657–660. <https://doi.org/10.1144/gsjgs.153.5.0657>.
- Worden, R.H., Armitage, P.J., Butcher, A.R., Churchill, J.M., Csoma, A.E., Hollis, C., Lander, R.H., Omma, J.E., 2018. Petroleum reservoir quality prediction: overview and contrasting approaches from sandstone and carbonate communities. *Geol. Soc. London Spec. Publ.* 435, 1–31. <https://doi.org/10.1144/SP435.21>.
- Yuan, G., Cao, Y., Gluyas, J., Li, X., Xi, K., Wang, Y., Jia, Z., Sun, P., Oxtoby, N.H., 2015. Feldspar dissolution, authigenic clays, and quartz cements in open and closed sandstone geochemical systems during diagenesis: typical examples from two sags in Bohai Bay Basin, East China. *AAPG Bull.* 99, 2121–2154.
- Yuan, G., Cao, Y., Schulz, H.-M., Hao, F., Gluyas, J., Liu, K., Yang, T., Wang, Y., Xi, K., Li, F., 2019. A review of feldspar alteration and its geological significance in sedimentary basins: from shallow aquifers to deep hydrocarbon reservoirs. *Earth Sci. Rev.* 191, 114–140.
- Zeng, L., 2010. Microfracturing in the upper triassic sichuan basin tight-gas sandstones: tectonic, overpressure, and diagenetic origins. *AAPG Bull.* 94, 1811–1825.